DE GRUYTER OPEN

Journal of ELECTRICAL ENGINEERING, VOL 68 (2017), NO6, 405–414

Modelling and control of solid oxide fuel cell generation system in microgrid

Niancheng Zhou, Chunyan Li, Fangqing Sun, Qianggang Wang*

Compared with other kinds of fuel cells, solid oxide fuel cell (SOFC) has been widely used in microgrids because of its higher efficiency and longer operation life. The weakness of SOFC lies in its slow response speed when grid disturbance occurs. This paper presents a control strategy that can promote the response speed and limit the fault current impulse for SOFC systems integrated into microgrids. First, the hysteretic control of the bidirectional DC-DC converter, which joins the SOFC and DC bus together, is explored. In addition, an improved droop control with limited current protection is applied in the DC-AC inverter, and the active synchronization control is applied to ensure a smooth transition of the microgrid between the grid-connected mode and the islanded mode. To validate the effectiveness of this control strategy, the control model was built and simulated in PSCAD/EMTDC.

K e y w o r d s: bidirectional DC-DC converter, fault current, microgrid, mode transition, solid oxide fuel cell (SOFC)

1 Introduction

Nowadays, distributed generations (DGs) have been increasingly applied in modern electrical distribution systems because of challenges, such as the increasing demand for energy, environmental problems, and increasing reliability of power systems [1, 2]. The high penetration levels of DGs cause problems, such as inverse power flow, voltage fluctuation, and protection problem in the distribution system. Microgrids, which contain a number of systematically organized DGs, different types of loads, and energy storage devices, have emerged as a framework to address these problems [3–7]. Microgrids are autonomous subsystems with control systems that provide guaranteed power quality for local loads. A microgrid provides local control and power quality support that allows for the integration of local resources and loads into the existing power grid and enables a high penetration of DGs.

Fuel cells are one of the suitable potential alternative DG sources for supplying electric energy to residential and commercial loads. Given the shortage of fossil fuel resources, clean fuel cells have been exploited and utilized to meet the energy needs due to their clean, quiet, and efficient specifications [8–10]. Compared with other kinds of fuel cells, solid oxide fuel cells (SOFCs) have more advantageous features, such as having no leakage, higher comprehensive utilization, and longer service life, among others. Consequently, SOFCs have become a key research field and attracted attention among researchers [11, 12].

Voltage-source inverters (VSIs) are normally used as power interfaces to set the frequency and voltage up to maintain the reliability of the operation of the local loads. Microgrids can operate either in grid-connected or islanded mode through the control of VSIs. In islanded mode, local loads such as hospital, apartments, economic centers, and universities, should be supplied by the DGs, whereas the loads are supplied by the grid in grid-connected mode. Many control strategies of VSIs have been investigated, where the droop control is considered a preferred option due to its flexibility. Although previous reports [13-15] studied a model of grid-connected SOFC generation power system whose voltage and frequency stability are supported by the grid, the control strategy of the inverter was not introduced. The control strategy for islanded mode is proposed in literature [16-18]. The control strategies without considering switching between the grid connection and islanded mode and the protection of the power electronic devices in microgrid. To address these problems, the present paper proposes a simple coordinated control method for smoothly transferring from islanded to grid-connected mode and protecting power electronic units in microgrid.

2 Modeling of SOFC power generation system

The configuration of the SOFC generation system along with its basic control structure is shown in Fig. 1. As shown in Fig. 1, the SOFC generation system contains an SOFC stack, a boost converter, a DC-AC inverter, a battery energy storage system (BESS), and a bi-directional DC-DC converter [19]. The primary power source is SOFC, which generates DC power. The boost converter can raise the DC voltage of SOFC to a stable value. The DC-AC inverter can detect the difference between the reference voltage and the output voltage to maintain the output voltage at the desired value. The storage battery is in parallel with the SOFC stack at the DC side of the inverter through the bi-directional DC-DC

* State Key Laboratory of Power Transmission Equipment and System Safety and New Technology, Chongqing University, 400044 Chongqing, China, qianggang1987@cqu.edu.c, cee$_n$czhou@cqu.edu.cn

DOI: 10.1515/jee-2017–0075, Print (till 2015) ISSN 1335-3632, On-line ISSN 1339-309X

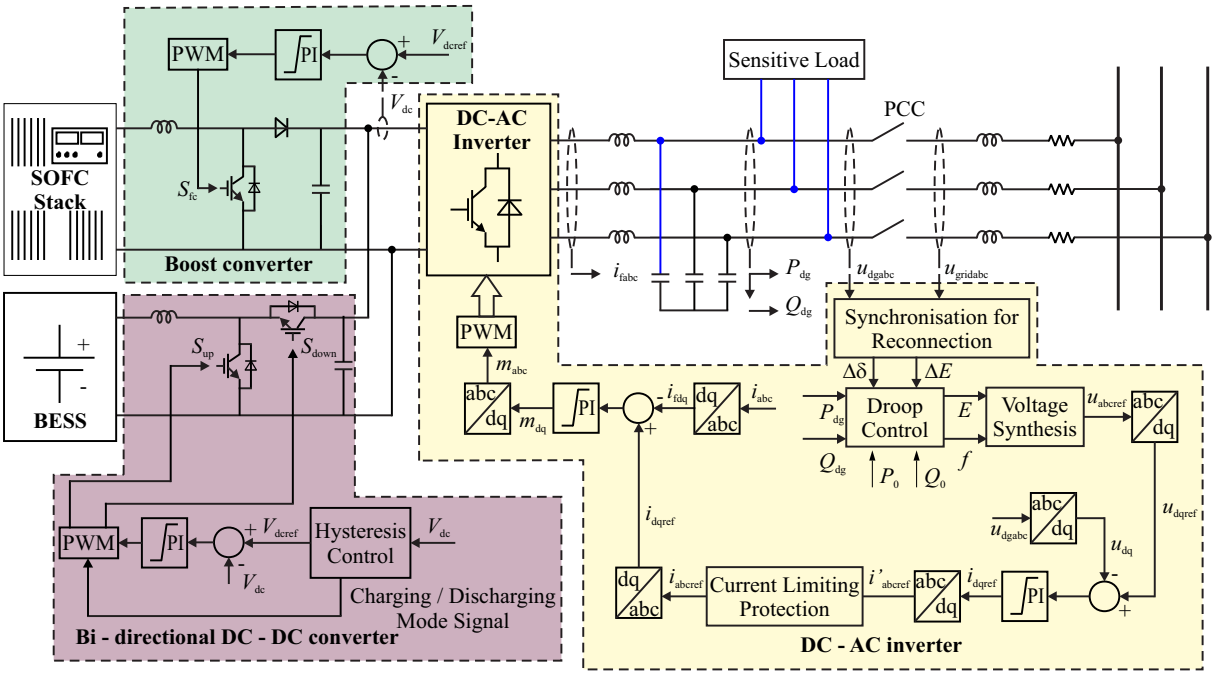

Fig. 1. Configuration of SOFC generation system along with its basic control structure

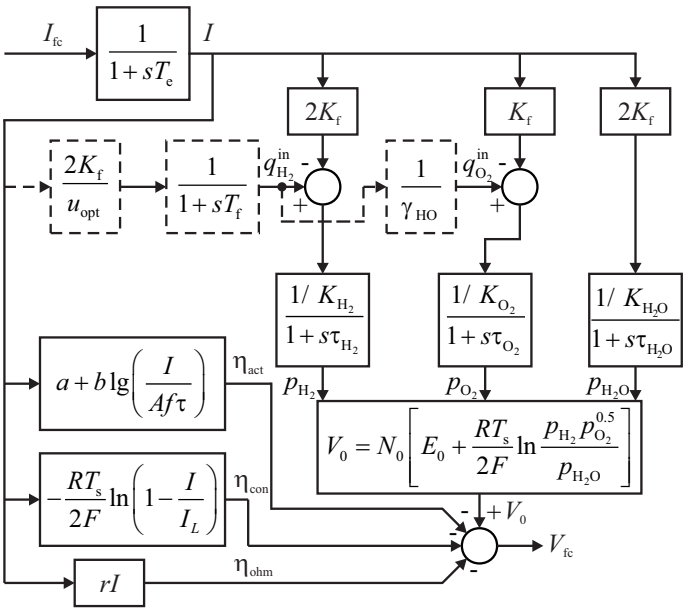

Fig. 2. SOFC stack dynamic model

converter, which is used to achieve the charging and discharging controls of the energy storage battery.

2.1 Modeling and Characteristics of SOFC stack

2.1.1 Modeling of SOFC stack

The different types of fuel cells are generally classified according to their electrolyte, which also determines their operating temperature. SOFC uses dense yttria-stabilized zirconia (YSZ), which is a solid ceramic material as its electrolyte. These cells operate at high temperature in the range of 800 °C to 1000 °C. Owing to its high efficiency, SOFCs are the most common types of fuel cells used in DG applications.

A single cell consists of an anode, a cathode, and solid oxide electrolyte. Oxidant reduction and fuel oxidation occur in the cathode and anode, respectively. Both poles contain a catalyst that accelerates the electrochemical reaction in the electrode. This catalyst is equivalent to a DC power supply, whose anode is the negative power supply and cathode is the positive power supply. The anode and cathode reactions of the SOFC are as follows

Anode reaction: $H_2 + O^{2-} \rightarrow H_2O + 2e^-$

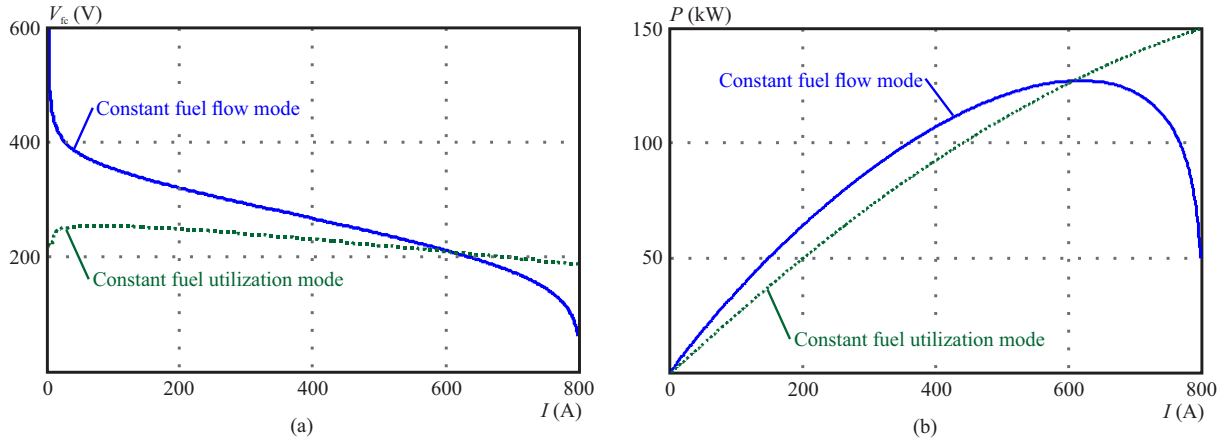

Fig. 3. $V-I$ and $P-I$ characteristics of open-loop SOFC at two different operation mode: (a) – V–I characteristics of open loop SOFC, (b) – P–I characteristics of open loop SOFC

Cathode reaction: $O_2 + 4e^- \rightarrow 2O^{2-}$

The fuel cell voltage is determined by chemical reactions because combustion does not occur in a fuel cell. The amount of the reaction enthalpy that can be converted to electricity in a fuel cell corresponds to Gibbs free energy. In this paper, the widely used SOFC dynamical model is taken as the study object, as shown in Fig. 2, [11, 12, 20] where V_{fc} is the stack output voltage, I_{fc} is the feedback signal current, I is the stack current, p_{H_2}, p_{O_2}, and $p_{\mathrm{H_2O}}$ are the pressure values of the hydrogen, the oxygen, and the water vapor in atm, respectively, E_0, η_{ohm}, η_{act}, and η_{con} represent the standard electromotive force, the ohmic polarization loss, the activation polarization loss, and the concentration polarization loss of the battery units, respectively, $q^{\mathrm{in}}_{\mathrm{O}_2}$ and $q^{\mathrm{in}}_{\mathrm{H}_2}$ are the input flows of oxygen and hydrogen (mol/s), respectively. Applying Nernsts equation, the SOFC stack output voltage V_{fc} is described as follows

$$V_{fc} = V_0 - \eta_{\mathrm{ohm}} - \eta_{\mathrm{con}} - \eta_{\mathrm{act}} \tag{1}$$

where

$$V_0 = N_0\left[E_0 + \frac{RT_s}{2F}\ln\frac{p_{\mathrm{H}_2}p^{0.5}_{\mathrm{O}_2}}{p_{\mathrm{H_2O}}}\right], \tag{2}$$

$$p_{\mathrm{H}_2} = \frac{1/K_{\mathrm{H}_2}}{1+\tau_{\mathrm{H}_2}s}\left(q^{\mathrm{in}}_{\mathrm{H}_2} - 2k_rI\right), \tag{3}$$

$$p_{\mathrm{O}_2} = \frac{1/K_{\mathrm{O}_2}}{1+\tau_{\mathrm{O}_2}s}\left(q^{\mathrm{in}}_{\mathrm{O}_2} - 2k_rI\right), \tag{4}$$

$$p_{\mathrm{H_2O}} = \frac{1/K_{\mathrm{H_2O}}}{1+\tau_{\mathrm{H_2O}}s}2k_rI\,, \tag{5}$$

$$\eta_{\mathrm{ohm}} = rI\,, \quad \eta_{\mathrm{con}} = -\frac{RT_s}{2F}\ln\left(1-\frac{I}{I_L}\right),$$

$$\eta_{\mathrm{act}} = a + b\lg\frac{I}{A_{fc}}. \tag{6}$$

The electrical response time in the fuel cells is generally fast and mainly associated with the speed of the chemical reaction that restores the charge drained by the load. Therefore, the first-order transfer function is a time constant (T_e, 0.8 s). The chemical response is associated with the time to change the chemical reaction parameters after a change in the flow of reactants. As such, the chemical response in the fuel processor is always slow. which stood by a first-order transfer function with a 5-s time constant (T_f). The hydrogen flow can be generated with stack current I, fuel efficiency u_{opt}, and hydrogen reaction coefficient K_r. Therefore, the oxygen flow can be obtained according to the oxygen-hydrogen ratio r_{HO}.

Two kinds of control mode for SOFCs exist: one is the constant fuel flow mode, and the other is the constant fuel utilization mode. For the constant fuel flow mode, the input fuel flow is constant and is not affected by the load current. In the constant fuel utilization mode, see the blocks with dotted lines in Fig. 2, T the rate of fuel utilization remains unchanged, and the load current is fed back to control the rate of fuel flow, which builds a link between the load and the fuel input quantity. In this paper, the constant fuel utilization mode is chosen as the control method of the SOFC model.

2.2.1 Characteristic Analysis of SOFC

The steady state characteristics (V–I and P–I characteristics) of the two control modes are shown in Fig. 3. In the constant fuel flow mode, the V–I characteristic of the SOFC is nonlinear.

In the constant fuel flow mode, the voltage drops at the low current region, which is dominated by activation loss. As the load current increases, the voltage drop is proportional to the current, where ohmic loss dominates. When the load current exceeds a certain value (760 A), the voltage drops sharply due to concentration loss. At the start, higher output power can be achieved at a higher load current, and a critical load current (600 A) is achieved when the output power reaches the maximum value. However, the voltage slope in the constant fuel utilization mode is lower than that in the constant fuel flow mode, and the output power shows an increasing trend with increasing current. This result can be attributed to the increased module between the input hydrogen and oxygen flow in

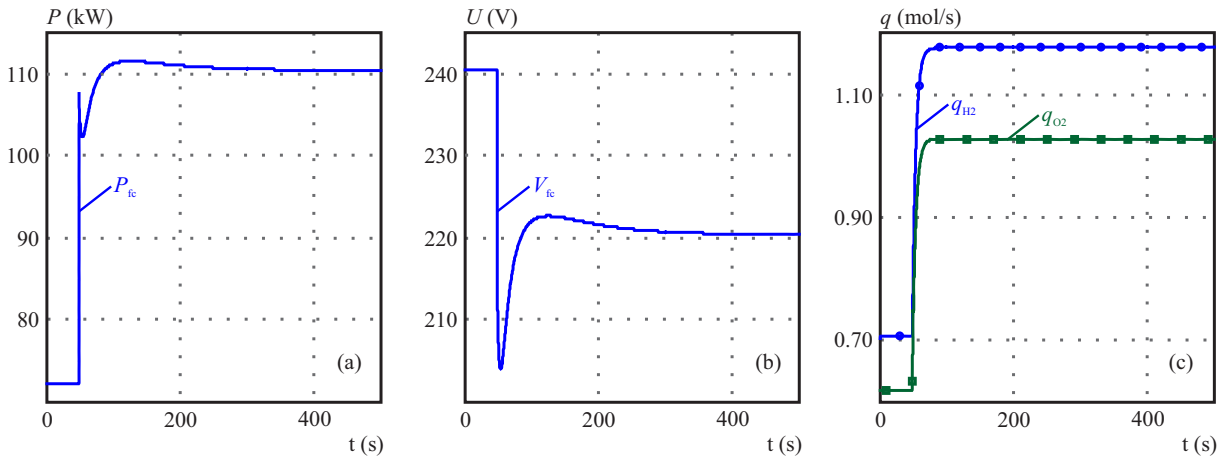

Fig. 4. Response of SOFC to stepwise current change (+200 A): (a) – voltage waveform, (b) – active power, (c) – input flow of hydrogen and oxygen

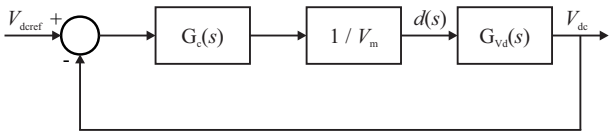

Fig. 5. Block diagram of the close-loop for the boost DC/DC converter

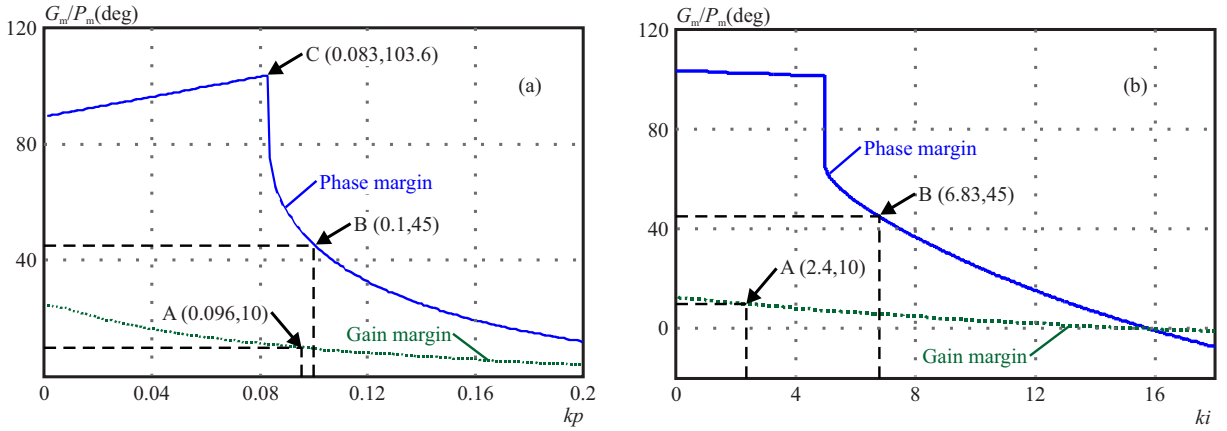

Fig. 6. Bode plot of the control loop of the boost DC/DC converter.(a) – changing k_p ($k_i = 1$), (b) – changing k_i ($k_p = 0.08$)

making the input hydrogen and oxygen flow, which can be increased in the same proportion. In practical applications, the flow of hydrogen and oxygen cannot infinitely increase; however, this paper does not consider this situation. According to Fig. 3, the V–I and the P–I curves of the SOFC model under the two control modes are consistent with the changing trends in literature [20], indicating that the SOFC model proposed in this paper can effectively and accurately reflect the internal characteristics of fuel cells.

Figure 4 shows the changing curves of the output voltage, power, input hydrogen, and oxygen flow under the constant fuel utilization mode when time is $t = 50$ s, and the load current jumps from 300 A to 500 A. As the load current has a step change, the hydrogen and oxygen flow both reach a new steady-state value within approximately 15 s, which are two parallel lines. This increment is due to the fact that the hydrogen and oxygen flows are determined by the feedback load current in the constant fuel utilization mode. As the load current increases, the voltage drops sharply, and then slowly increases to a new steady-state value, which can be attributed to the flow of hydrogen and oxygen reaching their new steady-state values. Simultaneously, the output power slowly increases to 110 kW value. Owing to the long chemical reaction time, the response times of voltage and power are slow, which takes nearly 200 s to fully reach the steady-state values.

2.2 Control of SOFC Power Generation System

Owing to the electrochemical properties of fuel cells, the output DC voltage shows a large variation range as the load or temperature changes. Therefore, a boost conversion is applied in the backward stage, which meets the DC bus voltage requirement and ensures the steady operations of the inverter. In the foregoing analysis, the power regulation speed of fuel cells is still too slow; thus, the control system cannot follow the rapid change of the

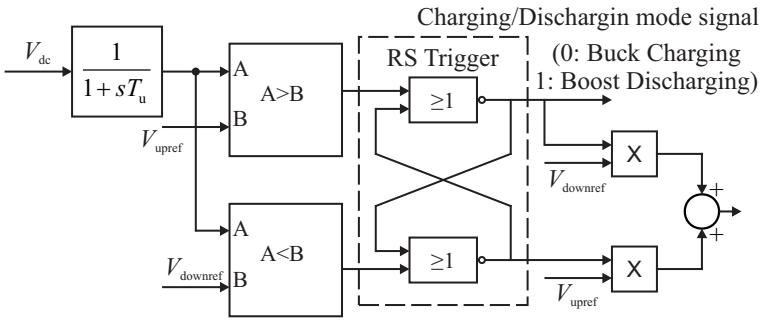

Fig. 7. Control block of voltage hysteresis-control strategy

load. Therefore, a storage battery, which is in parallel with the SOFC module at the DC side of the inverter, can reduce the system response time.

2.2.1 Boost Converter Control

The control system of the boost converter is shown in Fig. 1. The duty ratio can be obtained through the PI link with the DC voltage deviation signal, and the switch signal S_{fc} is generated from the PWM modulation. Figure 5 shows the block diagram of the closed-loop transfer function of the boost converter. A PI hysteresis compensation is used in the voltage feedback controlled function $G_c(s)$. Then, the open loop transfer function of the boost converter control system can be described as follows

$$G_{\mathrm{o}}(s) = \frac{G_c(s)G_{\mathrm{Vd}}(s)}{V_m} = \frac{k_p + \frac{k_i}{s}}{V_m} \frac{(1-D)V_{\mathrm{dcN}}\left[1 - \frac{sL}{(1-D)^2R}\right]}{LCs^2 + \frac{L}{R}s + (1-D)^2} \quad (7)$$

where $D = 1 - V_{\mathrm{fcN}}/V_{\mathrm{dcN}}$ is the duty ratio of the boost converter under rated operation condition (the subscript N stands for the rated value); L and C are the input inductance and the output capacitance, respectively; R is the equivalent resistance of the load; $V_m = 1.0$ is the sawtooth amplitude of the PWM modulator; and k_p and k_i are the parameters of the PI controller.

The phase margin and gain margin curves of the open-loop transfer function in the boost conversion system are shown in Fig. 6, where the curves change with k_p and k_i (detailed parameters in Tab. 1). In Figs. 6(a) and (b), A and B correspond to the gain margin $G_m = 10$ dB and phase margin $P_m = 45°$, respectively. The phase and gain margins show downward trends along with the increase of k_p and k_i. In Fig. 6(a), the phase margin begins to decline after the peak point C at $k_p = 0.083$. The system with a smaller stability margin has a bigger overshoot and a longer settling time. The parameters are set at $k_p = 0.08$ and $k_i = 2$ to ensure that the DC conversion has enough phase and gain margin.

2.2.2 Bi-directional DC-DC Converter Control

To improve the power regulation speed of SOFC system, the storage battery that operates as a fast responsor is in parallel with the fuel cells at the DC bus side through the bi-directional DC–DC converter. The topology structure of the bi-directional (buckboost) DC–DC converter is shown in Fig. 1.

Bi-directional DC/DC converter is used to ensure the voltage of DC bus to meet the inverters requirements. The parameter selection method for the voltage feedback PI control of bi-directional DC/DC converter is the same with that in Section 2.2.1. The charging/discharging frequency of the storage battery will influence its lifetime. In this paper, the hysteresis control strategy for the DC bus voltage is used. This control strategy helps to reduce the switching (charging/discharging) times and improve the lifetime of the whole system. Figure 7 shows the block diagram of the voltage hysteresis control mode, and time constant T_u of the low-pass filtering link is set as 0.02 s. The procedure for the judging are as follows

Step 1: Compare the DC voltage with the reference voltage (V_{upref} & V_{downref}). If the dc voltage $V_{dc} = V_{\mathrm{upref}}$, please proceed to Step 2; else if $V_{dc} = V_{\mathrm{downref}}$, please proceed to Step 3; if $V_{\mathrm{downref}} < V_{dc} < V_{\mathrm{upref}}$, please proceed to Step 4.

Step 2: Operate on charging mode. If $V_{dc} = V_{\mathrm{upref}}$, the output of charging/discharging mode signal is 0, and DC converter works in buck mode with power switch Sup shutting off and S_{down} working, as shown in Fig. 4.

Step 3: Operate on discharging mode. If $V_{dc} = V_{\mathrm{downref}}$, the output of charging/discharging mode signal is 1. DC converter works in boost mode with power switch S_{dowm} shutting off and S_{up} working, as shown in Fig. 4.

Step 4: Operating mode concurs with the initial state. That is, the mode is charging mode when the initial state is charging mode, or the mode is discharging mode when the initial state is discharging mode.

In this paper, the setting value of V_{downref} and V_{upref} are 780 and 820 V, respectively.

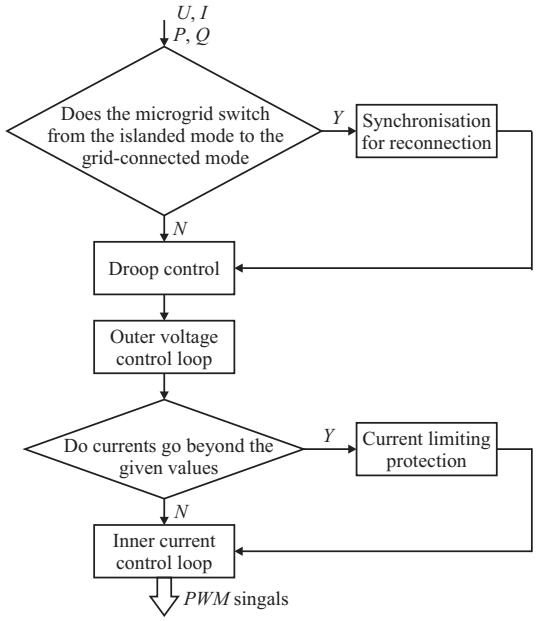

Fig. 8. Control flowchart of the DC-AC inverter

2.2.3 DC-AC Inverter Control

As shown in Fig. 8, the controller contains the outer voltage control loop, the inner current control loop, and the real and reactive power control loops. In theory, the flow of real power P between the two nodes can be controlled by varying the supply frequency, whereas the flow of reactive power Q can be controlled by changing the voltage magnitude. Using these concepts, this section proposes a droop control with "real power versus supply frequency P–f" and "reactive power versus voltage Q–E" droop characteristics.

To allow for the normal operations of the SOFC system and the smooth switching between the two modes (*ie*, grid-connected and islanded modes of the microgrid), E–f droop control strategy is used in the DC–AC inverter. The droop characteristics are shown as follows

$$\begin{aligned} f &= f_0 - m(P_0 - P_{dg})\,, \\ E &= E_0 - n(Q_0 - Q_{dg}) \end{aligned} \tag{8}$$

where P_{dg} and Q_{dg} are the active and reactive powers of the SOFC generation system, respectively; P_0, Q_0, f_0, and E_0 are the active and reactive reference powers, the rated frequency, and the voltage at point of common coupling (PCC) when the microgrid is under grid-connected mode, respectively [21].

Figure 9 shows the droop characteristic, and the P–f and Q–E droop slopes m and n can be calculated as follows

$$m = \frac{f_0 - f_{\min}}{P_0 - P_{\max}}\,, \quad n = \frac{E_0 - E_{\min}}{Q_0 - Q_{\max}} \tag{9}$$

where $f_{\min}$ and $E_{\min}$ are the minimum allowable frequency and voltage at PCC, and $P_{\max}$, and $Q_{\max}$ are the maximum active and the reactive powers, respectively.

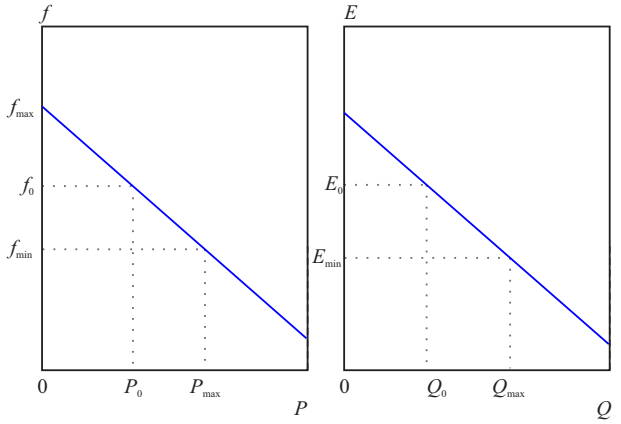

Fig. 9. Droop characteristic

By reasonably setting the droop coefficients, we can ensure that the change in output voltage magnitude and frequency of SOFC system is minimal under different operation conditions. The synchronization block for safe reconnection between the microgrid and the large power system is shown in Fig. 1. The voltage amplitude deviation ΔE and phase deviation $\Delta\delta$, the correcting signals of both sides of PCC, are compensated to the output references E and f in droop control to realize synchronization in advance [22].

In Fig. 1, the double closed loop control (*ie*, inner current and outer voltage controls) are used in the DC–AC inverter. A current limiting protection is set in the inner current loop, which effectively limits the inverters fault current (Fig. 10).

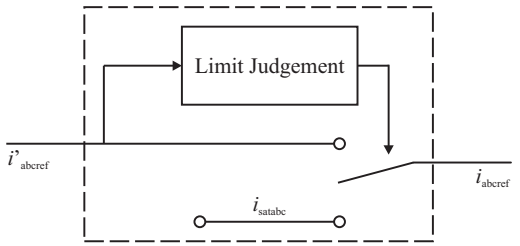

Fig. 10. Current limiting protection

The reference dq axis current i_{dqref} of the outer voltage loop will be evaluated to determine whether the current exceeds the limitation after park transformation. Once the output current exceeds the given limit, the three-phase reference current will be limited to a saturation current i_{satabc}. The amplitude of the saturation current is a given value, and the phase must be determined according to the power control strategy of the inverter system. In this research, the phase of the saturation current should be the same with grid voltage. In addition, the limit current amplitude is 1.5 times larger than that of the rated current. The current limit control not only helps to avoid the damage to the power switch caused by the excessive instantaneous current, but also allows the microgrid system to revert to normal operational conditions once faults are cleared.

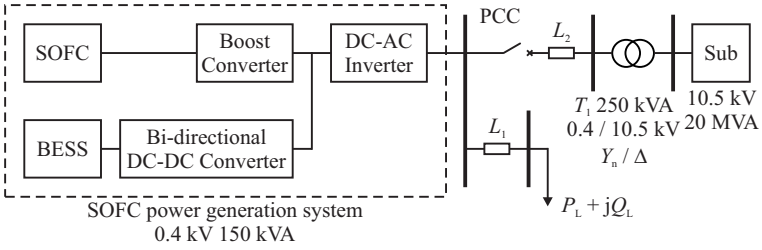

Fig. 11. Microgrid structure

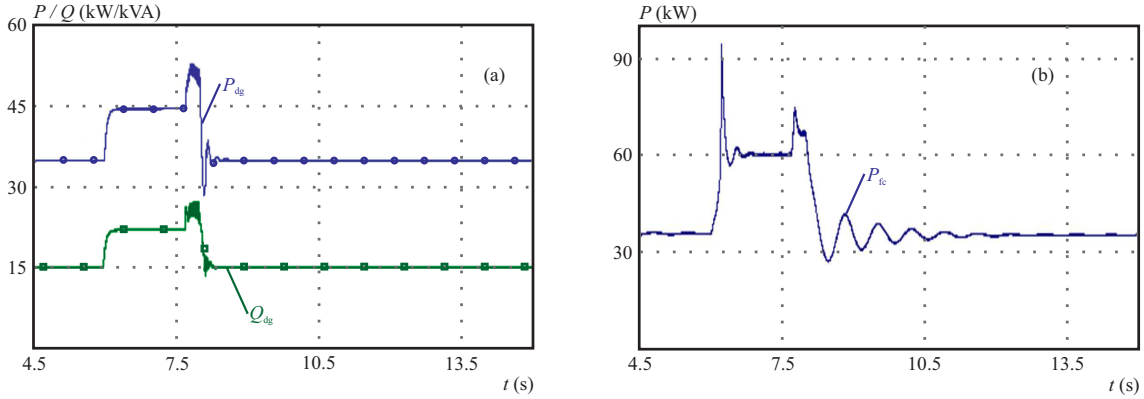

Fig. 12. Output power of generation system and SOFC stack : (a) – generation system , (b) – SOFC stack

Table 1. Parameters of the microgrid containing the SOFC generating system

	Variable	Value	Unit
Boost converter	L_{fc}	0.6	mH
	C_{fc}	3000	μF
	k_p	0.08	–
	k_i	0.2	–
Bi-directional DC-DC converter	L_{bess}	3	mH
	k_p	0.1	–
	k_i	1.2	–
DC-AC Inverter	m	0.04	Hz/kW
	n	0.36	V/kVar
	L_f	0.9	mH
	C_f	250	μF
Lines	Z_L	$0.642 + j0.083$	Ω/km
	L_1	3	Km
	L_2	1	Km

3 Results of simmulation

The microgrid model is established in PSCAD/EMTDC (shown as Fig. 11), and the system parameters are shown in Table 1. Based on the microgrid model, this paper studies the dynamic simulations under the grid-connected mode, the islanded mode, and the transition process.

3.1 Transition between grid - connected and islanded modes

At $t = 6$ s, the microgrid switches from grid-connected mode to islanded mode. Under the islanded mode, SOFC serves the microgrid and the storage battery automatically charges and discharges through the bi-directional DC–DC converter. Their output powers match each other to guarantee a stable power supply for the microgrid At $t = 7.7$ s, the voltage amplitude and phase of the microgrid side at PCC begin to synchronize with the main system .At $t = 8$ s, the microgrid reverts to the grid-connected mode.

Figure 12(a) shows the changes of the output power of the SOFC power generation system from $t = 6$ s (when the system disconnects from the power grid) to $t = 8$ s (when the system reconnects to the grid). Under the grid-connected mode, the local load of the microgrid can absorb a part of the power from the main grid. However, when the local load switches to islanded mode, the microgrid cannot obtain power from the large power grid, and thus, the fuel cells have to increase their output power to meet the local load needs. Therefore, after decoupling and turning into the islanded mode, the output active and reactive powers of the SOFC generation system increase, and the output power P_{fc} of the SOFC stacks increases as well, as shown in Fig. 12. However, the variation tendency of the output active power of the SOFC generation system is gentler during the transition process due to the smoothing effect of the power electronic devices.

When the microgrid switches its operation mode, the frequency of the system voltage changes, as shown in Fig. 13. Under the islanded mode, without the support of the large power grid, the islanded microgrid is still able to operate in a stable manner, owing to the interaction between the SOFC stacks and the storage battery. Furthermore, the microgrid frequency decreases slightly based on the active power increment and the droop coefficients. Meanwhile, in the reconnection and synchroniza-

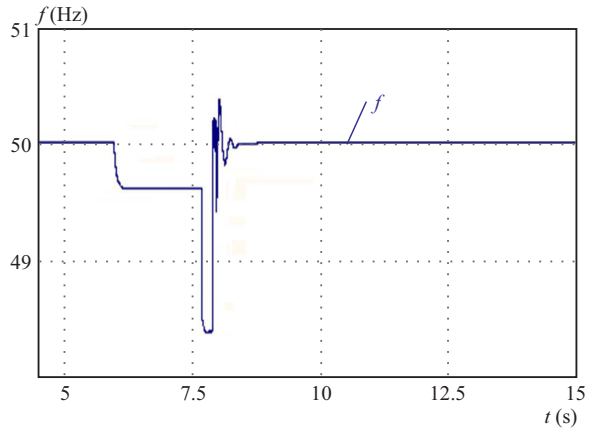

Fig. 13. Frequency response when switching from islanded mode to grid - connected mode

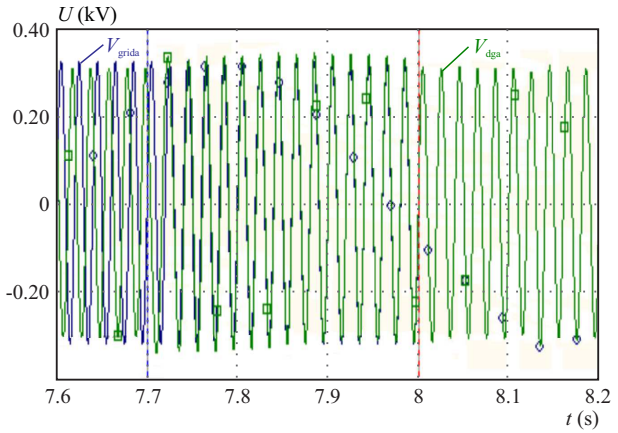

Fig. 14. Synchronization progress of voltage magnitude and phase at PCC

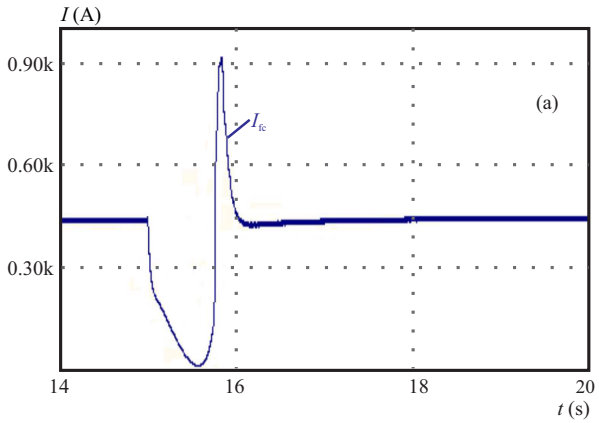

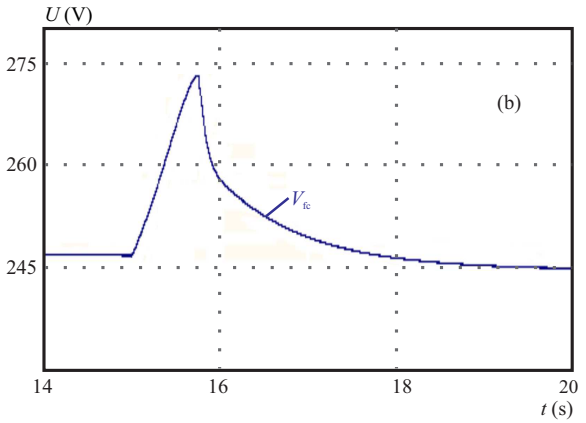

Fig. 15. Current and voltage of SOFC stack when subjected to a fault : (a) – current waveform, (b) – voltage waveform

tion process, the frequency drops for a short period at the beginning of the synchronous process, given that the origin values of the phase angle deviation $\Delta\delta$ between both sides of the PCC is negative. As shown in Fig. 14, after a 0.3-s synchronous process, the voltage phase and amplitude of the PCC on the microgrid side remains consistent with those on the main grid side. After a smooth reconnection, the output power of the SOFC drops back to the level before the islanded mode.

3.2 Fault Characteristics

When the microgrid is operating on islanded mode, a three-phase short circuit fault occurs at the load node when $t = 15$ s. At $t = 15.5$ s, the fault is cleared, and the system returns to the normal operating state. This paper studies the dynamic characteristics of the fuel cells and the overall system during this process.

Figure 15 shows the stack current and voltage. The stack current of the SOFC cell suddenly drops to 0 when the fault occurs. When the fault is cleared, the current first rises up and then decreases and reverts to the initial state. When the fault occurs at the load node on islanded mode, the loads suddenly drop to 0. Given that the voltage of the fuel cells changes slowly due to the longer chemical response time as compared with the transient response time, the current of the fuel cells declines and reaches 0. Then, the current of fuel cells returns to the normal state after the fault is cleared. Simultaneously, the voltage slightly increases from 245 V to 272 V.

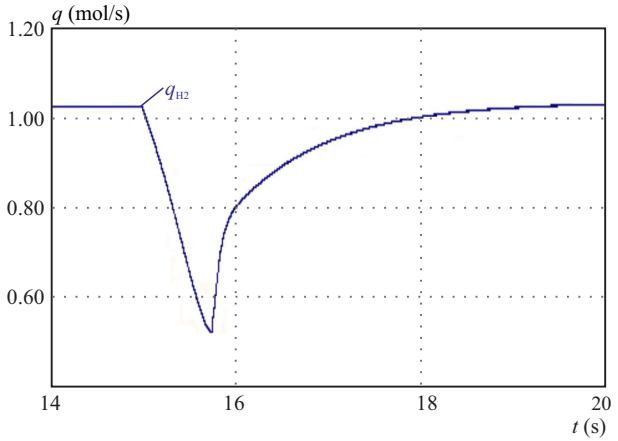

Fig. 16. Hydrogen flow when subjected to a fault

Figure 16 shows that the input hydrogen flow $q_{\mathrm{H2}}^{\mathrm{in}}$ of the SOFC drops substantially from 1.02 mol/s to nearly 0.53 mol/s at $t = 15$ s when the fault occurs. After $t = 15.5$ s when the fault is cleared, the input hydrogen flow gradually rises to 1.02 mol/s. The input hydrogen flow decreases slowly according to the two first-order transfer

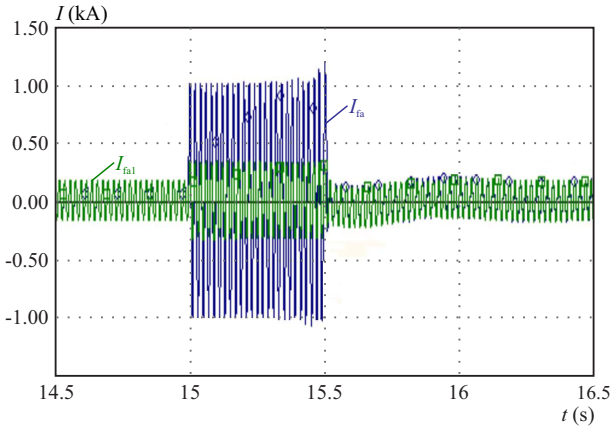

Fig. 17. Output current of the inverter before and after the installation of current limit protection

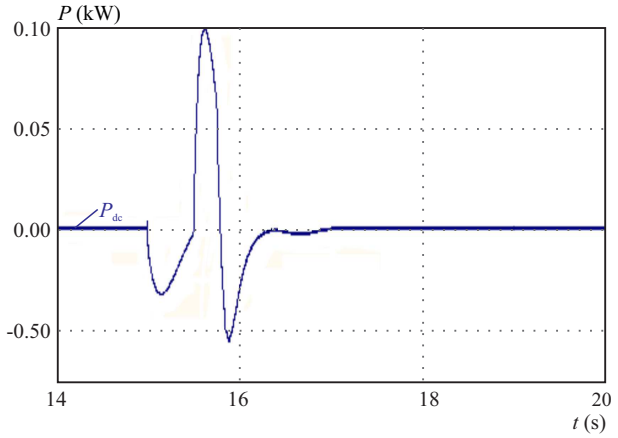

Fig. 18. Power of the battery at fault

functions, which indicate the electrical and the chemical response times, as shown in Fig. 2. Hence, before the input hydrogen flow drops to 0, the fault is cleared and input hydrogen flow reverts to normal value.

When the three-phase short circuit fault occurs, the DC voltage and the current of the SOFC change considerably, which will then affect the SOFC stacks and the quality and life of the fuel cells. Under the three-phase short circuit fault, the inner loop current of the inverter suddenly exceeds the limit value given by the current limit protection link. Then, the current limit protection takes effect.

Figure 17 shows the output current curves of the SOFC system under two conditions: the green line represents the output current for the system with a current limit protection link, while the blue line stands for the current without current limit protection. The current-limit protection is found to act rapidly at 15 s when the short circuit fault occurs. When operating without the current-limit protection, the inverter current will be twice as large as the rated current, and thus, the inverter must be cut off to protect electronic devices.

During the fault, the storage battery operates under Buck charging mode due to the rise of the DC bus voltage. Meanwhile, when the fault is clearing at the start, the storage battery works under boost discharging mode to quickly compensate for the insufficient output power of the fuel cell stacks. Figure 18 shows that the DC voltage rises beyond $V_{\text{upref}} = 820$ V at $t = 15$ s when the fault occurs, and then, the storage battery begins charging. After the occurrence of the fault, the DC voltage drops below $V_{\text{downref}} = 780$ V, and the storage battery begins to discharge. Then, after a short period of being charged, the storage battery finally returns to the standby state.

4 Conclusion

A complete control scheme designed for the SOFC power generation system operating under two modes (*ie*, the constant fuel utilization mode and the constant fuel flow mode) was presented in this paper. First, the hysteresis control strategy for the DC bus voltage was proposed. The control coefficients are then selected according to the trend curves of the phase and the gain margins of the open loop transfer function. Finally, the dynamic response of the SOFC was increased through this strategy. In addition, the V/f droop control with limiting current protection is designed and applied in the DC–AC inverter. This control effectively limits the fault current and ensures a smooth transition of the microgrid between the grid-connected and the islanded modes. Through the simulation test, the model is proven to precisely reflect the chemical properties of the SOFC, and the control strategy of the SOFC helps the microgrid operate in a stable manner under different conditions.

Acknowledgements

This work was supported by the Fundamental Research Funds for the Central Universities (106112016CDJXY150001).

References

[1] B. Belvedere, M. Bianchi, A. Borghetti *et al*, "A Microcontroller-Based Power Management System for Standalone Microgrids with Hybrid Power Supply", *IEEE Transactions on Sustainable Energy*, vol. 3, pp. 422–431, 2012.

[2] G. Liu, Y. Xu and K. Tomsovic, "Bidding Strategy for Microgrid Day-Ahead Market Based on Hybrid Stochastic/Robust Optimization", *IEEE Transactions on Smart Grid*, vol. 7, pp. 227–237, 2016.

[3] F. Katiraei, R. Iravani, N. Hatziargyriou *et al*, "Microgrids management", *IEEE Power & Energy Magazine*, vol. 6, pp. 54–65, 2008.

[4] S. A. Taher, M. Zolfaghari, C. Cho *et al*, "A New Approach for Soft Synchronization of Microgrid Using Robust Control Theory", *IEEE Transactions on Power Delivery*, vol. 32, pp. 1370–1381, 2017.

[5] M. Hamzeh, M. Ghafouri, H. Karimi *et al*, "Power Oscillations Damping DC Microgrids", *IEEE Transactions on Energy Conversion*, vol. 31, pp. 970–980, 2016.

[6] N. Nikmehr and S. Najafi-Ravadanegh, "Optimal Operation of Distributed Generations Micro-Grids under Uncertainties Load

and Renewable Power Generation Using Heuristic Algorithm", *IEt Renewable Power Generation*, vol. 9, pp. 982–990, 2015.

[7] K. T. Tan, P. L. So, Y. C. Chu *et al*, "Coordinated Control and Energy Management of Distributed Generation Inverters a Microgrid", *IEEE Transactions on Power Delivery*, vol. 28, pp. 704–713, 2013.

[8] W. Du, H. F. Wang, X. F. Zhang *et al*,"Effect of Grid-Connected Solid Oxide Fuel Cell Power Generation on Power Systems Small-Signal Stability", *IET Renewable Power Generation*, vol. 6, pp. 24–37, 2012.

[9] S. F. Yang, C. S. Hwang, C. H. Tsai *et al*, "Production of Metal-Supported Solid Oxide Fuel Cell Using Thermal Plasma Spraying Technique", *IEEE Transactions on Plasma Science*, vol. 45, no. 2, pp. 318–322, 2017.

[10] S. Obara, "Control of Cyclic Fluctuations an Independent Microgrid by an SOFC Triple Combined Cycle Inertia System", *International Journal of Electrical Power & Energy Systems*, vol. 68, pp. 89-102, 2015.

[11] Xu, Dezhi, Bin, Jiang and Fei Liu, "Improved Data Driven Model Free Adaptive Constrained Control for a Solid Oxide Fuel Cell", *IET Control Theory & Applications*, vol. 10, pp. 1412–1419, 2016.

[12] Yigeng Huangfu, Fei Gao and A. Abbas-Turki, "Transient Dynamic and Modeling Parameter Sensitivity Analysis of 1D Solid Oxide Fuel Cell Model", *Energy Conversion and Management*, vol. 17, pp. 172–185, 2013.

[13] T. Zhang and G. Feng, "Rapid Load Following of a SOFC Power System via Stable Fuzzy Predictive Controller", *IEEE Transaction Fuzzy System*, vol. 17. pp. 357–371, 2009.

[14] E. M. Stewart, R. Tumilty, J. Fletcher, A. Lutz, G. Ault and J. McDonald, "Analysis of a Distributed Grid-Connected Fuel Cell during Fault Conditions", *IEEE Transaction Power System*, vol. 25, pp. 497–505, 2010.

[15] S. Fedakar, S. Bahceci and T. Yalcinoz, "Modeling and Simulation of Grid Connected Solid Oxide Fuel Cell Using PSCAD", *Journal of Renewable & Sustainable Energy*, vol. 6, pp. 16–361, 2014.

[16] A. Ghazanfari, M. Hamzeh, H. Mokhtari *et al*, "Active Power Management of Multihybrid Fuel Cell/Supercapacitor Power Conversion System a Medium Voltage Microgrid", *IEEE Transactions on Smart Grid*, vol. 3, pp. 1903–1910, 2012.

[17] X. Sun, B. Liu, Y. Cai *et al*, "Frequency-Based Power Management for Photovoltaic/Battery/Fuel Cell-Electrolyser Stand-Alone Microgrid", *Iet Power Electronics*, vol. 9, pp. 2602–2610, 2016.

[18] Y. Han, P. Shen, X. Zhao *et al*, "Control Strategies for Islanded Microgrid Using Enhanced Hierarchical Control Structure with Multiple Current-Loop Damping Schemes", *IEEE Transactions on Smart Grid*, vol. 8, pp. 1139–1153, 2017.

[19] M. Ramezani, S. Li and Y. Sun, "Combining Droop and Direct Current Vector Control for Control of Parallel Inverters Microgrid", *IET Renew. Power Gener.*, vol. 11, pp. 107–114, 2017.

[20] C. Wang and M. H. Nehrir, "Short-Time Overloading Capability and Distributed Generation Applications of Solid Oxide Fuel Cells", *IEEE Transactions on Energy Conversion*, vol. 22, pp. 898–906, 2007.

[21] Y. W. Li and C. N. Kao, "An Accurate Power Control Strategy for Inverter Based Distributed Generation Units Operating a Low Voltage Microgrid", *Energy Conversion Congress and Exposition*, pp. 3363–3370, 2009.

[22] Y. Li, D. M. Vilathgamuwa and P. C. Loh, "Design, Analysis, and Real-Time Testing of a Controller for Multibus Microgrid System", *IEEE Trans. Power Electron.* , vol. 19, pp. 1195–1204, 2004.

Received 5 June 2017

Niancheng Zhou was born in Chongqing, China in 1969 and obtained his BS, MS, and PhD degrees in electrical engineering from Chongqing University, Chongqing, China, in 1991, 1994, and 1997, respectively. He worked at Chongqing Kuayue Technology Company, Ltd., Chongqing from 1997 to 2003. He is currently a professor at the College of Electrical Engineering, Chongqing University. He was a research fellow at Nanyang Technological University, Singapore from 2010 to 2011. His current research interests include the analysis and operation of power systems, microgrids, and power quality.

Chunyan Li was born in Henan, China, in 1985 and obtained her MS degree in electrical engineering in 2011 from Chongqing University, Chongqing, China, where she is currently pursuing a PhD degree in electrical engineering. Her current research interests include power system operation, microgrids, and relay protection.

Fangqing Sun was born in Shandong, China, in 1991 and obtained her BS degree in electrical engineering from Northeast Electric Power University, Jilin, China in 2014. She is currently pursuing an MS degree in Chongqing University, Chongqing, China. Her current research interests include power system operation and power quality.

Qianggang Wang was born in Fujian, China, in 1987 and obtained his BS and PhD degrees from Chongqing University, Chongqing, China in 2009 and 2015, respectively. Since 2015, he has been a lecturer at the School of Electrical Engineering, Chongqing University. Currently, he is a research fellow at Nanyang Technological University, Singapore. His research interests include power system operation, microgrids, and power quality.